ACS OMEGA

http://pubs.acs.org/journal/acsodf

Article

Extraction of Fulvic Acid from Lignite and Characterization of Its Functional Groups

Guanqun Gong,[§] Liangwei Xu,[§] Yingjie Zhang,* Weixin Liu, Ming Wang, Yufeng Zhao, Xin Yuan, and Yajun Li

Cite This: *ACS Omega* 2020, 5, 27953−27961

Read Online

ACCESS | Metrics & More | Article Recommendations

ABSTRACT: Fulvic acid (FA) is a complex organic mixture composed of small molecules. The structure and composition of FA vary greatly because of the different raw materials used for preparing FA. In this work, FA was extracted from shallow low-rank lignite by hydrogen peroxide (H_2O_2) in a microwave field, and the functional groups of FA were characterized. The optimal extraction process was determined, with the H_2O_2 concentration being the key factor affecting the yield of FA. Thermogravimetric analysis showed that FA was mainly composed of low molecular weight and readily pyrolyzed compounds. As shown by Fourier transform infrared spectroscopy, in the process of FA extraction by H_2O_2 oxidation of lignite, the content of −COOH increased, long-chain aliphatic compounds decreased, stretching vibrations of aromatic ring skeletons disappeared, and aromatic ring substitution became mainly tri- or disubstitution. Fluorescence spectroscopy indicated that FA had a low degree of aromaticity. X-ray photoelectron spectroscopy qualitatively and quantitatively revealed that the main modes of carbon−oxygen bonding in FA were C−O−, COO−, and C═O. Thus, this study not only lays a foundation for studying the composition and structure of coal-based FA but also opens a new avenue for a clean and efficient utilization of lignite.

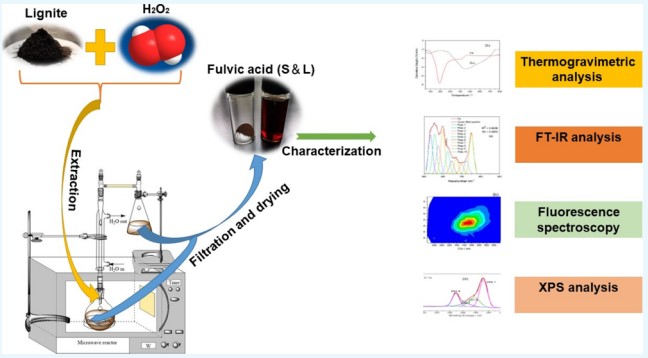

1. INTRODUCTION

Humus is a complex polydisperse polymer mixture with diverse structures and aggregation states, which is widely distributed in natural soils, water, and minerals. It is mainly composed of C, O, H, and N, in which the proportion of organic carbon is generally between 40 and 60%.[1−4] According to its source, humus can be divided into soil humus, aquatic humus, and mineral humus. According to its composition and structure, humus can be divided into fulvic acid (FA), humic acid (HA), and humin. Among these three components of humus, FA is the alkali- and acid-soluble component, HA is the alkali-soluble and acid-insoluble component, and humin is the insoluble residue.[5−7]

FA has a low molecular weight of only a few hundred Daltons. It can have a wide range of pH values. Because of its unique physical and chemical properties, FA has been used in a wide range of fields including agriculture, medicine, environment, and materials. In agriculture, FA can significantly improve the morphological characteristics of crops as well as their seed and straw yields. In addition, chelation of FA with metals can regulate metal absorption by crops, thereby affecting the growth and metabolism of plants.[8−10] As a donor or recipient with a variety of biomedical functions, FA can promote electrochemical balance, stimulate immune regulatory molecules, and induce apoptosis of cancer cells.[11,12] Compared with HA, FA contains a more diverse range of functional groups, has a higher degree of humization, and is more stable in the chemical and biological adsorption of some heavy metals.[13] FA-based electrospun hard carbon nanofibers (PF−CNF) have been applied as negative electrodes of sodium ion batteries, where cycling 100 times at 100 $mA{\cdot}g^{-1}$ current density resulted in a capacity retention rate of 91%; this indicated that FA-based carbon nanomaterials have excellent cycling performance.[14]

The conventional extraction method for FA and HA is alkali dissolution and acid precipitation. First, humus in the raw material is extracted by NaOH or KOH, and then the pH is adjusted with HCl or HNO_3 to obtain an FA solution.[15−18] However, because of the introduction of high concentrations of Na^+ and K^+ in the extraction process, it is difficult to obtain pure FA by this method. Additionally, as large volumes of acid

Received: July 16, 2020
Accepted: September 25, 2020
Published: October 22, 2020

https://dx.doi.org/10.1021/acsomega.0c03388
ACS Omega 2020, 5, 27953−27961

Table 1. Comparison of Different Extraction Methods of FA

method	principle	equipment	time	advantages	disadvantages
alkali-soluble acid precipitation[23,24]	solubility differences	conventional extractor	5−6 h	easy to operate	time-consuming
					low extraction yield
					high content of impurities
chemical degradation[25,26]	oxidation increases acid solubility	conventional extractor	36−72 h	high yielding	time-consuming
					expensive
ultrasound-assisted[27]	ultrasound energy	ultrasonic water bath	1 h	rapid	lower efficiency than the microwave method
					range of ultrasonic action is narrow
microwave-assisted[28]	microwave energy	microwave extractor	10−20 min	very rapid	difficult to industrialize

and alkali are used in this process, it is not an environmentally friendly method. Natural organic matter has been used to synthesize FA, with a composition similar to natural FA, but as the process is complex and the raw materials hard to obtain, this approach has not become popular.[19] Recent studies have shown that the oxidation of coal increases the yields of FA and HA, and the macromolecular structure of coal is greatly affected by free radical chain reactions in the oxidation process.[20] Among the oxidation methods, nitric acid not only increased the yield of HA from 20 to 85%, but also obtained FA and HA with low molecular weight and low aromaticity.[21] However, nitric acid treatment is expensive, and pre-oxidation by H_2O_2 causes some weak covalent bonds in coal to break and introduces oxygen functional groups; this is similar to the effect of treatment with nitric acid, but high concentrations of H_2O_2 are not conducive to the formation of FA and HA.[22] Different methods of extracting FA are compared in Table 1.

Lignite is a type of inferior fuel with abundant reserves and rich organic matter, but with high moisture and ash content and low calorific value, it produces very high levels of pollutants in direct combustion. Therefore, the conversion of lignite into value-added chemicals or liquid fuel under mild conditions is of great value. For example, lignite has been used as a raw material for the effective production of FA.[29−34] In this paper, FA was extracted from lignite using H_2O_2 in a microwave field, with a focus on exploring the optimal process conditions and investigating the composition and structure of the resulting FA. FA was analyzed and characterized by thermogravimetric (TG) analysis, Fourier transform infrared spectroscopy (FT-IR), fluorescence spectroscopy, and X-ray photoelectron spectroscopy (XPS) to provide theoretical and technical support for the production of high-purity FA products.

2. RESULTS AND DISCUSSION

2.1. Extraction of FA from Lignite. The effects of microwave power, reaction time, the concentration of H_2O_2, and the ratio of oxygen to coal on the yield of FA were investigated using an orthogonal experimental design. The L9 (3^4) orthogonal array was used, with the factors and levels shown in Table 2 and the experimental results shown in Table 3.

Table 3 shows that the yield of FA in the fifth group of experiments was the highest, at 30.55%. As a higher K value indicates higher priority, with $K_{A3} > K_{A2} > K_{A1}$, A_3 was the optimal level for factor A; and, by the same token, B_2, C_3, and D_2 were the optimal levels for factors B, C, and D, respectively. Therefore, the optimal level combination for FA was $A_3B_2C_3D_2$; under these conditions, the oxygen−coal ratio was 11, the H_2O_2 concentration was 21%, the microwave power was 400 W, and the reaction time was 10 min. Because the experimental combination of $A_3B_2C_3D_2$ was not included in the orthogonal experimental scheme, the $A_3B_2C_3D_2$ combination was tested three times with an average FA yield of 31.67%.

Table 2. Orthogonal Experiment Factors and Levels for FA Extraction Using H_2O_2[a]

	factor			
level	A	B	C	D
1	9	18	200	8
2	10	21	300	10
3	11	24	400	12

[a]Note: A—oxygen−coal ratio; B—H_2O_2 concentration/%; C—microwave power/W; D—time/min.

Table 3. Orthogonal Experiment Results and Range Analysis for FA Extraction Using H_2O_2

	factor				
number	A	B	C	D	yield/%
1	9	18	200	8	23.55
2	9	21	300	10	28.17
3	9	24	400	12	29.82
4	10	18	300	12	24.04
5	10	21	400	8	30.55
6	10	24	200	10	27.19
7	11	18	400	10	28.67
8	11	21	200	12	30.12
9	11	24	300	8	27.03
K_1	27.180	25.420	26.953	27.043	
K_2	27.260	29.613	26.413	28.010	
K_3	28.607	28.013	29.680	27.993	
R	1.427	4.193	3.267	0.967	

As shown in Table 3, the range analysis results of $R_B > R_C > R_A > R_D$ showed that the order of influence of the four factors was H_2O_2 concentration > microwave power > oxygen−coal ratio > reaction time. Orthogonal test results with different parameters are shown in Figure 1, which indicates that increasing the oxygen−coal ratio and microwave power could promote the extraction of FA. When the concentration of H_2O_2 was too high, the large amounts of $^{\bullet}HO$ and O_2^- produced may have oxidized and decomposed the generated FA, resulting in its decreased yield.[35] Figure 1 also shows that with oxygenolysis of the shallow low-rank lignite (SLL), the yield of FA first increased, but as H_2O_2 did not oxidize the lignite continuously, the yield stabilized.

https://dx.doi.org/10.1021/acsomega.0c03388
ACS Omega 2020, 5, 27953−27961

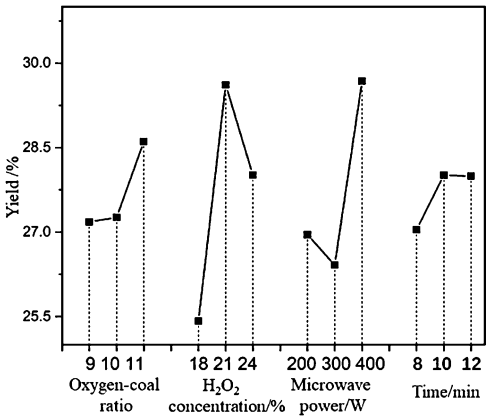

Figure 1. Yields of FA under orthogonal experimental conditions.

2.2. Elemental Analysis. As shown in Table 4, the content of C and H in FA was significantly lower than in SLL, while the content of O was significantly higher. The ratios of C to H and C to O in FA were less than 1. The main reason for this was that, under the microwave field, H_2O_2 destroyed weak covalent bonds such as R−O−R, R−OH, α-H, and so forth. In SLL, this resulted in the cleavage of fatty side chains and other substituents, and many oxygen-containing hydrogen-rich groups were introduced into the molecular structure; alternatively, small oxygen- and hydrogen-rich molecules were formed, such as C═O, −OH, and −COOH, from fragments of the broken alkyl chains.[22]

Table 4. Elemental Analysis of SLL and FA[a]

	elemental analysis (W %, daf)					molar ratio	
sample	C	H	N	S	O*	C/H	C/O
SLL	76.20	4.25	1.7	0.39	17.46	1.49	5.82
FA	40.22	3.81	1.82	0.22	53.93	0.88	0.99

[a]Note: *determined by subtraction.

The content of N increased, while S decreased, indicating that microwaves combined with H_2O_2 could regulate the structure of N- and S-containing components in SLL coal, but whether these components were inorganic salts in SLL or organic molecular structural elements of SLL and FA needs to be further verified.[36]

2.3. TG Analysis. The pyrolysis behavior of SLL and FA at 0−800 °C is shown in Figure 2. The temperature range of 50−100 °C was a common region for SLL and FA, where drying and dehydration occurred. As can be seen from Figure 2a, the weight loss for both SLL and FA was less than 5% at this stage, as water adsorbed on the surface of SLL and FA surface evaporated[37] with increasing temperature. Figure 2b shows that the weight loss rate of the FA increased rapidly after 75 °C, indicating that the loss of small molecular substances present in its structure began to accompany the moisture removal. As shown in Figure 2a, from 100−300 °C, the weight loss of SLL was only 4.7%, but FA lost more than 40% weight. The derivative TG (DTG) curve shows a maximum weight loss peak for FA near 200 °C, which was about 250 °C lower than the maximum weight loss peak for SLL (Figure 2b). This showed that FA contained many volatile small molecular compounds with poor thermal stability. At about 400 °C, a nonsignificant weight loss peak appeared in the FA DTG curve, which may have been caused by bridge bond fracture and the decomposition of most oxygen-containing functional groups. At 500 °C, the weight loss rate of FA was basically unchanged at 65% (Figure 2b), which was much higher than that of SLL (Figure 2a); this was because the content of readily pyrolyzed substances in FA was higher than in SLL.[38] When the temperature exceeded 600 °C, the pyrolysis reaction entered the final stage.[39]

2.4. FT-IR Analysis. The types and relative content of functional groups in SLL and FA were studied by using qualitative and semi-quantitative FT-IR analysis methods. The IR spectra of SLL and FA were fitted and analyzed in detail by Peakfit V4.12. R^2 and SE were used to measure the fitting effect. In order to obtain a better fitting effect, four regions of SLL were fitted and three regions of FA were fitted. Absorption peaks corresponding to functional groups are shown in Figures 3 and 4, and the relative contents of functional groups in each region are shown in Tables 5 and 6. The absorption peaks of SLL and FA could be divided into aromatic ring substituents from 900 to 660 cm^{-1}, oxygen-containing functional groups from 1900 to 1000 cm^{-1}, aliphatic alkyl groups from 3000 to 2700 cm^{-1}, and hydroxyl functional groups from 3600 to 3000 cm^{-1}.[40,41]

Phenolic, alcohol, and carboxylic acid hydroxyl groups were the main types of hydroxyl groups, as shown in Tables 5 and 6 (3600−3000 cm^{-1}). Because of the moisture in the sample, the spectral value of alcohol hydroxyl groups was larger than the actual hydroxyl content in SLL and FA. Figure 4c shows that, near 3030 and 3014 cm^{-1}, FA had a moderate energy band corresponding to −OH stretching vibrations on −COOH. It

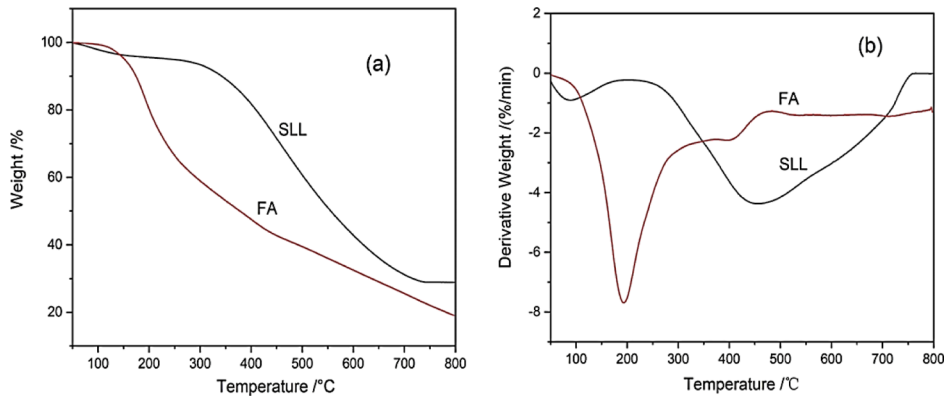

Figure 2. (a) TG and (b) DTG curves of SLL and FA.

https://dx.doi.org/10.1021/acsomega.0c03388
ACS Omega 2020, 5, 27953−27961

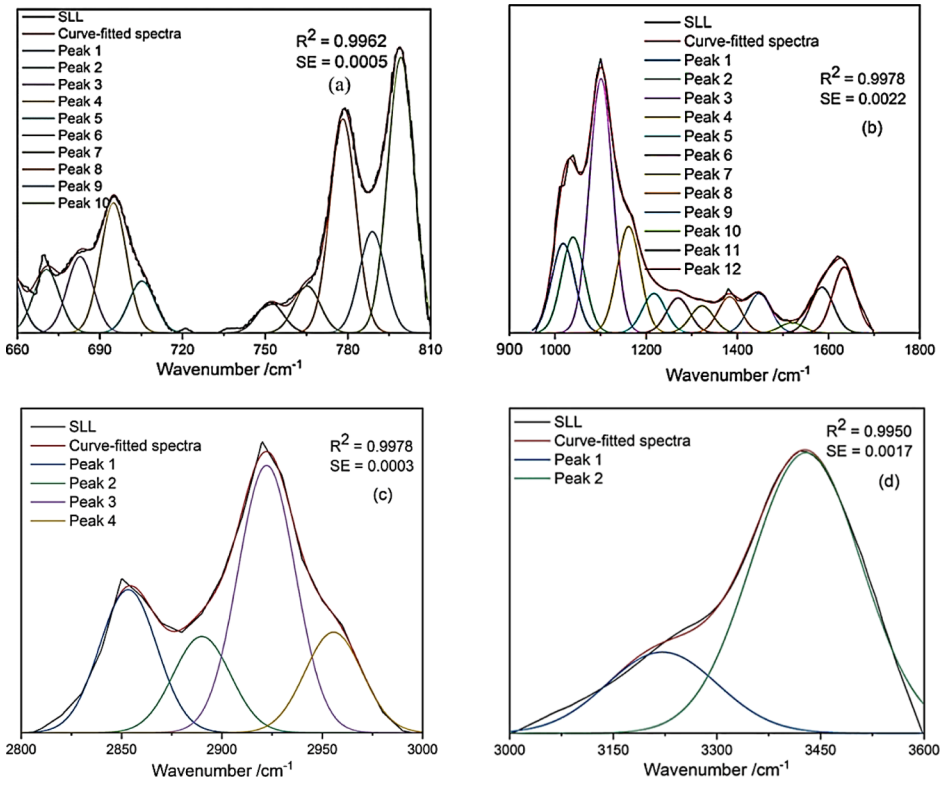

Figure 3. FT-IR spectrum peak fitting curves for SLL: (a) 660−810; (b) 900−1800; (c) 2800−3000; and (d) 3000−3600 cm^{-1}.

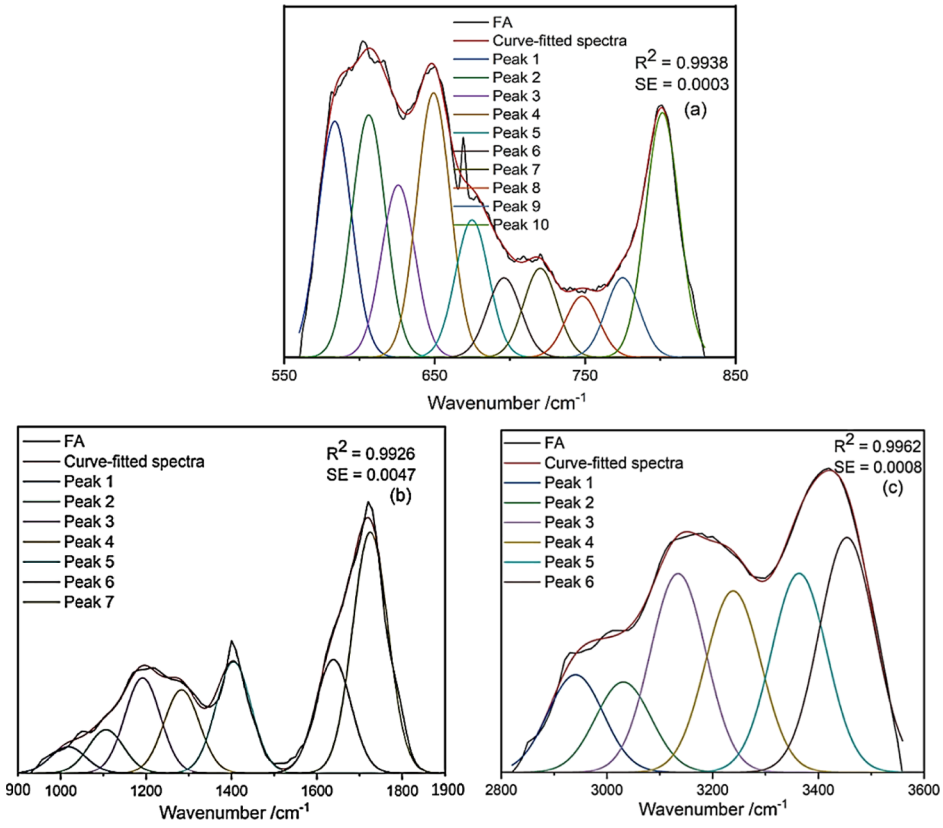

Figure 4. FT-IR spectrum peak fitting curves for FA: (a) 550−850; (b) 900−1900; and (c) 2800−3600 cm^{-1}.

was determined that the SLL hydroxyl groups were mainly phenolic (77.58%), as were the FA hydroxyl groups (43.3%), but FA also contained a considerable proportion of carboxylic acid hydroxyl groups (28.85%).

https://dx.doi.org/10.1021/acsomega.0c03388
ACS Omega 2020, 5, 27953−27961

Table 5. FT-IR Spectrum Peak Attributions for SLL

wavenumber range/cm^{-1}	peak number	wavenumber/cm^{-1}	area/%	attribution
3600−3000	1	3429	77.58	phenolic hydroxyl
	2	3220	22.42	alcohol hydroxyl
3000−2800	1	2955	16.55	RCH_3 symmetric stretching
	2	2922	44.03	$R_1CH_2R_2$ anti-symmetric stretching
	3	2889	15.85	RCH_3 symmetric stretching
	4	2853	23.57	$R_1CH_2R_2$ symmetric stretching
1700−900	1	1634	7.79	COO− anti-symmetric stretching
	2	1585	5.40	aromatic ring skeleton
	3	1519	1.20	aromatic ring skeleton
	4	1448	4.65	aromatic ring skeleton
	5	1383	4.28	C−O on phenol
	6	1322	3.20	C−O on phenol
	7	1270	4.12	C−O on phenyl ether
	8	1217	4.66	C−O on phenol
	9	1161	12.61	C−O on phenyl ether
	10	1100	30.14	C−O on aliphatic ether
	11	1039	11.35	C−O on acid anhydride
	12	1017	10.60	C−O on aliphatic ether
810−660	1	799	25.93	tri-substituted aromatics
	2	788	9.52	tri-substituted aromatics
	3	778	20.13	tri-substituted aromatics
	4	765	4.14	di-substituted substitutions
	5	751	2.86	di-substituted aromatics
	6	705	4.87	mono-substituted aromatics
	7	694	12.25	mono-substituted aromatics

Table 6. FT-IR Spectrum Peak Attributions for FA

waverange/cm^{-1}	peak number	wavenumber/cm^{-1}	area/%	attribution
3600−2800	1	3454	23.44	phenolic hydroxyl
	2	3363	19.86	phenolic hydroxyl
	3	3238	18.11	alcohol hydroxyl
	4	3134	19.84	hydroxyl on carboxylic acids
	5	3030	9.01	hydroxyl on carboxylic acids
	6	2940	9.74	RCH_3 stretching vibration
1890−850	1	1725	33.79	C═O on carboxylic acids
	2	1638	15.91	COO− anti-symmetric stretching vibration
	3	1405	15.56	C−O on hydroxyl
	4	1283	11.66	C−O on phenyl ether
	5	1191	13.33	C−O on aliphatic ether
	6	1106	6.06	C−O on aliphatic ether
	7	1017	3.68	C−O on acid anhydride
830−690	1	801	15.23	tri-substituted aromatics
	2	774	4.96	di-substituted aromatics
	3	748	3.81	di-substituted aromatics
	4	720	5.54	di-substituted aromatics
	5	696	4.95	mono-substituted aromatics

The aliphatic structure forms a bridge bond to connect the aromatic part of the molecular structure and various functional groups. As shown in Table 5 (3000−2700 cm^{-1}), RCH_3 and $R_1CH_2R_2$ were the main components of the aliphatic structure in SLL, as indicated by their stretching vibrations. It was inferred that the peaks at 2922 and 2853 cm^{-1} corresponded to $R_1CH_2R_2$ anti-symmetric stretching and symmetrical stretching, respectively, and 2889, 2955, and 2940 cm^{-1} corresponded to symmetrical stretching of RCH_3. In SLL, the ratio of $R_1CH_2R_2$ anti-symmetric stretching to symmetric stretching was 1.871 and the ratio of $R_1CH_2R_2$ to RCH_3 was 2.09.

As shown in Tables 5 and 6 (1900−1000 cm^{-1}), the oxygen-containing functional groups of SLL and FA were mainly carboxyl, acid anhydride, and ether moieties. It can be seen from Figures 3b and 4b that there was a strong energy band corresponding to COO− anti-symmetric stretching vibrations near 1630 cm^{-1}. For FA, carboxylic acid C═O groups appeared at 1725 cm^{-1} with a relative content of 33.79%, which indicated that there were more carboxyl groups in FA than in SLL. Aliphatic ethers and phenyl ethers are two important types of ethers, and their ratios were 2.44:1 and 1.66:1 for SLL and FA, respectively; thus, the relative content of aliphatic and phenyl ethers was lower in FA than in SLL,

https://dx.doi.org/10.1021/acsomega.0c03388
ACS Omega 2020, 5, 27953−27961

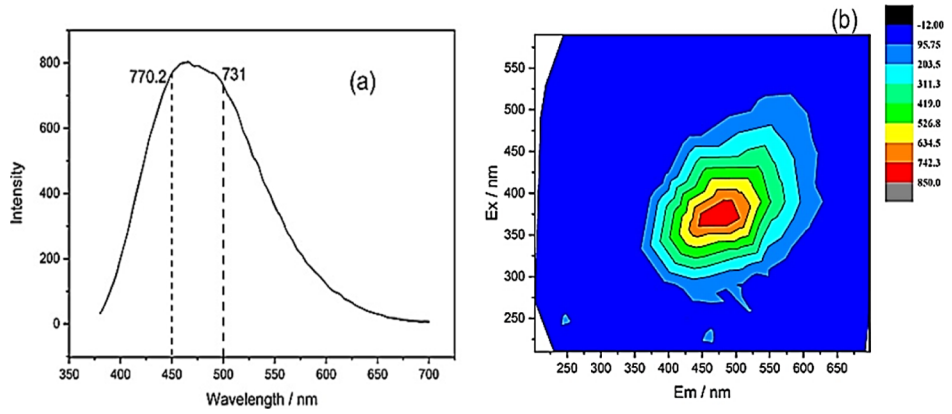

Figure 5. (a) Fluorescence emission spectrum and (b) three-dimensional excitation emission matrix fluorescence spectrum contour map of FA.

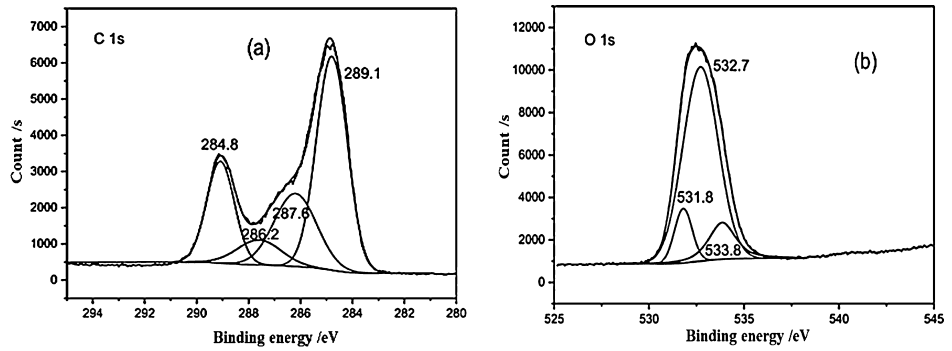

Figure 6. (a) C 1s and (b) O 1s spectra of FA.

which could be explained by the cleavage of C−O bridge bonds during oxygen hydrolysis.

It is also worth noting that aromatic ring skeleton vibrations appeared near 1448, 1519, and 1585 cm^{-1} in SLL, which showed that SLL had stronger aromaticity than FA. The aromatic moieties of SLL and FA were examined via their characteristic peaks from 900 to 600 cm^{-1}. Tables 5 and 6 show that both SLL and FA had aromatic rings with tri-, di-, and mono-substitution, with relative content of 55.58, 7.00, and 17.12% in SLL, respectively, and 15.23, 14.31, and 4.95% in FA, respectively. Thus, tri-substitution was the main substitution pattern in SLL, while FA mainly had tri- or di-substituted aromatic rings.

Results of FT-IR analysis showed that in the process of extracting FA by H_2O_2 oxidation of SLL, the content of −COOH, aliphatic alkyl groups decreased, long-chain aliphatic structures decreased, stretching vibrations of aromatic ring skeletons disappeared, and aromatic ring substitution was mainly tri- and di-substitution.

Compared with the structure of FA obtained by alkali-soluble acid precipitation (FA_1), microwave-assisted H_2O_2 had a better oxygen hydrolysis effect on macromolecules and aromatic structures in the SLL. FA had fewer aromatic structures and lower molecular weight and had stronger absorption peaks than FA_1 at 1660 and 1081 cm^{-1}. The band at 1660 cm^{-1} was attributed to the C═C vibrations of aromatic structures, conjugated with C═O. The band at 1081 cm^{-1} was attributed to C−O stretching, indicating the presence of polysaccharide or polysaccharide-like compounds.[24,28] Compared with FA obtained without H_2O_2 oxygenolysis (FA_2), FA had a wider band near 1100 cm^{-1} arising from tensile vibrations of C−O. This indicated that the oxygenation process with H_2O_2 increased the content of C−O.[23]

2.5. Fluorescence Spectroscopy. As shown in Figure 5a, there was a strong fluorescence peak at 465 nm and the fluorescence intensity reached 804. This indicated that the complex structure of FA was composed of a variety of groups with fluorescent characteristics, and the superposition of multiple peaks led to the high intensity and wide shape of the fluorescence peak. The fluorescence index ($f_{450/500}$) refers to the ratio of the fluorescence intensities emitted by the sample at 450 and 500 nm when the fixed excitation wavelength was 370 nm, which reflects the aromaticity of the structure.[42] As this value is negatively correlated with aromaticity, the $f_{450/500}$ value of 1.05 indicated that FA has low aromaticity.

The three-dimensional fluorescence spectrum of FA is shown in Figure 5b. It was clear that FA had only one fluorescence peak, positioned at $\lambda_{Ex/Em}$ = 360−393/443−498 nm. The peak appeared similar to an HA fluorescence peak, and it was considered that the appearance of the peak was related to the rich carboxyl and carbonyl groups in the material structure. This confirmed the presence of many carboxyl and carbonyl groups in FA.[43]

2.6. XPS Analysis. Data were fitted and analyzed in detail by Peakfit V4.12 (Figure 6). According to the XPS C 1s data given in Table 7, of the four forms in which carbon was found on the FA surface, the highest content was carbon in the form of C−H and C−C, corresponding to binding energy of 284.8 eV, and the relative content was 48.5%. This was followed by carbon in the form of C−O−, including C−OH and C−O−C, with a total relative content of 22.7%. The content of carbon in the form of COO− was slightly less than that of C−O,

https://dx.doi.org/10.1021/acsomega.0c03388
ACS Omega 2020, 5, 27953−27961

Table 7. XPS Results for FA, Including Binding Energies, fwhm, and Relative Percentages (Area)

	binding energy/eV	fwhm/eV	area/%	compound
C 1s	284.8	1.4	48.5	C−C, C−H
	286.2	1.9	22.7	C−O
	287.6	2.0	8.1	C═O
	289.1	1.3	20.7	COO−
O 1s	531.8	1.1	10.6	C═O
	532.7	2.2	75.9	C−O−
	533.8	1.6	13.5	COO−

accounting for about 20%, indicating that FA contained a large proportion of COO−. There was least C═O carbon in FA, only 8.1%, indicating that C═O carbon made up only a small amount relative to the content of COO− carbon.

The oxygen elements identified via XPS O 1s mainly existed in three forms: C═O, C−O, and COO−. The relative content of C−O was the highest at 75.9%, followed by COO−, and then C═O, confirming the XPS C 1s results, which indicated that FA contains more C−O and COO− than C═O.

3. CONCLUSIONS

With the assistance of microwave energy, high-yield FA was obtained by oxidation of SLL with H_2O_2. Elemental analysis, TG analysis, and FT-IR showed that $^{\bullet}OH$ and O_2^- produced by H_2O_2 caused SLL to undergo aromatic ring opening under the microwave field, destroying the long alkyl chains and aromatic structure of SLL. The obtained FA had low aromaticity and short molecular chains and was rich in functional groups such as −COOH and C−O. Fluorescence spectroscopy and XPS showed that the content of oxygen-containing functional groups in FA was C−O > −COO > C═O. Compared with the traditional method of extracting FA with alkali and acid, this process has advantages of a high extraction yield, environmentally friendly reagents, and process simplicity. Through characterization, it was determined that coal-based FA is a low molecular weight substance rich in −COOH and C−O. This work provides an effective method for the efficient utilization of low-rank coal and lays a foundation for in-depth understanding of coal-based FA molecules.

4. EXPERIMENTAL SECTION

4.1. Materials and Methods. Reagents were all analytically pure, and the mass fraction of H_2O_2 was 30%. The coal sample was SLL from the eastern mining area of Inner Mongolia, which was dried at 80 °C for 24 h.

SLL (2 g) and a certain concentration H_2O_2 solution were placed in a microwave chemical reactor to react at a certain microwave power. The reaction mixture was then filtered, and the filtrate was concentrated by a rotary evaporator. The concentrated filtrate was dried in a blast drying box at 60 °C to obtain solid FA. The yield of FA was calculated according to eq 1, where η is the yield of FA, m_1 is the mass of FA, and m_0 is the mass of SLL.

$$\eta = \frac{m_1}{m_0} \times 100\% \quad (1)$$

The source of SLL and the reaction device are shown in Figure 7. The FA obtained was purified by the sulfuric acid-acetone method.[40]

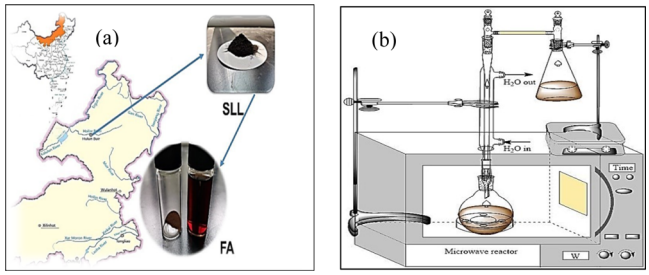

Figure 7. (a) Coal and FA (solid and liquid) samples and (b) reaction device.

4.2. Characterization. Elemental analysis was performed using a Kaiyuan 5e-CHN2000 and 5E-S3200, and the fluorescence index of FA was measured using a Hitachi F4600 fluorescence spectrophotometer with a fixed excitation wavelength of 370 nm. The state of C and O on the surface of FA was determined by photoelectron spectroscopy using a Thermo Fisher ESCALAB 250Xi X-ray photoelectron spectrometer. TG and DTG curves of SLL and FA at the heating rate of 5 min/°C were measured by a Netzsch TG−DSC synchronous thermal analyzer. Infrared spectra of SLL and FA were measured on a Bruker VERTEX 80v Fourier transform infrared spectrometer, and the infrared spectrum data between 500 and 4000 cm^{-1} were obtained.

AUTHOR INFORMATION

Corresponding Author

Yingjie Zhang − *Key Laboratory of Coal Processing and Efficient Utilization of Ministry of Education, Xuzhou 221116, China; School of Chemical Engineering & Technology, China University of Mining and Technology, Xuzhou 221116, China;* orcid.org/0000-0002-7850-006X; Email: zhangcumt123@126.com

Authors

Guanqun Gong − *Key Laboratory of Coal Processing and Efficient Utilization of Ministry of Education, Xuzhou 221116, China; School of Chemical Engineering & Technology, China University of Mining and Technology, Xuzhou 221116, China;* orcid.org/0000-0001-7896-9477

Liangwei Xu − *School of Chemical Engineering & Technology, China University of Mining and Technology, Xuzhou 221116, China*

Weixin Liu − *School of Chemical Engineering & Technology, China University of Mining and Technology, Xuzhou 221116, China*

Ming Wang − *School of Chemical Engineering & Technology, China University of Mining and Technology, Xuzhou 221116, China*

Yufeng Zhao − *School of Chemical Engineering & Technology, China University of Mining and Technology, Xuzhou 221116, China*

Xin Yuan − *School of Chemical Engineering & Technology, China University of Mining and Technology, Xuzhou 221116, China*

Yajun Li − *School of Chemical Engineering & Technology, China University of Mining and Technology, Xuzhou 221116, China*

Complete contact information is available at: https://pubs.acs.org/10.1021/acsomega.0c03388

https://dx.doi.org/10.1021/acsomega.0c03388
ACS Omega 2020, 5, 27953−27961

Author Contributions

§G.G. and L.X. contributed equally to this work and both of them are the co-first author.

Notes

The authors declare no competing financial interest.

■ ACKNOWLEDGMENTS

This work was supported by the National Nature Science Foundation of China (grants 21776299 and 21576281), China Coal Industry Association Scientific and Technological Guidance Project (grants MTKJ2015-220 and MTKJ2012-288), and China University of Mining and Technology teaching reform project for postgraduate education (2019YJSJG043, YJSJG-2018-01). The authors are grateful to Advanced Analysis & Computation Center, China University of Mining and Technology for providing the testing services for this work.

■ REFERENCES

(1) Piccolo, A. *Dissolved Humus in Soil Waters*; Piccolo, A., Ed.; Elsevier Science B.V.: Amsterdam, 1996.
(2) Zhang, A.; Zhang, Y. J.; Zheng, H. L.; Ma, L. L.; Liu, W. J.; Gong, G. Q. Study on the extraction of fulvic acid from lignite by microwave-assisted hydrogen peroxide. *Int. J. Oil Gas Coal Technol.* **2018**, *18*, 146−162.
(3) Doskočil, L.; Grasset, L.; Válková, D. Hydrogen peroxide oxidation of humic acids and lignite. *Fuel* **2014**, *134*, 406−413.
(4) Zsolnay, A. *Dissolved Humus in Soil Waters*; Piccolo, A., Ed.; Elsevier Science B.V.: Amsterdam, 1996.
(5) Rodríguez, F. J. Characterization of aquatic humic substances. *Water Environ. J.* **2011**, *25*, 163−170.
(6) Amir, S.; Hafidi, M.; Merlina, G.; Revel, J.-C. Structural characterization of fulvic acids during composting of sewage sludge. *Process Biochem.* **2005**, *40*, 1693−1700.
(7) Klencsár, Z.; Köntös, Z. EPR analysis of Fe(3+) and Mn(2+) complexation sites in fulvic acid extracted from lignite. *J. Phys. Chem. A* **2018**, *122*, 3190−3203.
(8) Abdel-Baky, Y. R.; Abouziena, H. F.; Amin, A. A.; Elsh, M. R. Improve quality and productivity of some faba bean cultivars with foliar application of fulvic acid. *Bull. Natl. Res. Cent.* **2019**, *43*, 1−11.
(9) Ali, S.; Bharwana, S. A.; Rizwan, M.; Farid, M.; Kanwal, S.; Ali, Q.; Ibrahim, M.; Gill, R. A.; Khan, M. D. Fulvic acid mediates chromium (Cr) tolerance in wheat (Triticum aestivum L.) through lowering of Cr uptake and improved antioxidant defense system. *Environ. Sci. Pollut. Res.* **2015**, *22*, 10601−10609.
(10) Priya, B. N. V.; Mahavishnan, K.; Gurumurthy, D. S.; Bindumadhava, H.; Ambika, P.; Sharma, N. K. Fulvic acid (FA) for enhanced nutrient uptake and growth: insights from biochemical and genomic studies. *J. Crop Improv.* **2014**, *28*, 740−757.
(11) Ali, S.; Rizwan, M.; Waqas, A.; Hussain, M. B.; Hussain, A.; Liu, S.; Alqarawi, A. A.; Hashem, A.; Abd Allah, E. F. Fulvic Acid Prevents Chromium-induced Morphological, Photosynthetic, and Oxidative Alterations in Wheat Irrigated with Tannery Waste Water. *J. Plant Growth Regul.* **2018**, *37*, 1357−1367.
(12) Jayasooriya, R. G. P. T.; Dilshara, M. G.; Kang, C.-H.; Lee, S.; Choi, Y. H.; Jeong, Y. K.; Kim, G.-Y. Fulvic acid promotes extracellular anti-cancer mediators from RAW 264.7 cells, causing to cancer cell death in vitro. *Int. Immunopharmacol.* **2016**, *36*, 241−248.
(13) Rashid, I.; Murtaza, G.; Zahir, Z. A.; Farooq, M. Effect of humic and fulvic acid transformation on cadmium availability to wheat cultivars in sewage sludge amended soil. *Environ. Sci. Pollut. Res.* **2018**, *25*, 16071−16079.
(14) Zhao, P.-Y.; Zhang, J.; Li, Q.; Wang, C.-Y. Electrochemical performance of fulvic acid-based electrospun hard carbon nanofibers as promising anodes for sodium-ion batteries. *J. Power Sources* **2016**, *334*, 170−178.
(15) Tsuda, K.; Mori, H.; Asakawa, D.; Yanagi, Y.; Kodama, H.; Nagao, S.; Yonebayashi, K.; Fujitake, N. Characterization and grouping of aquatic fulvic acids isolated from clear-water rivers and lakes in Japan. *Water Res.* **2010**, *44*, 3837−3846.
(16) Jiang, T.; Han, G.; Zhang, Y.; Huang, Y.; Li, G.; Guo, Y.; Yang, Y. Improving extraction yield of humic substances from lignite with anthraquinone in alkaline solution. *J. Cent. S. Univ. Technol.* **2011**, *18*, 68−72.
(17) Gondar, D.; Lopez, R.; Fiol, S.; Antelo, J. M.; Arce, F. Characterization and acid−base properties of fulvic and humic acids isolated from two horizons of an ombrotrophic peat bog. *Geoderma* **2005**, *126*, 367−374.
(18) Baigorri, R.; Fuentes, M.; Gonzàlez-Gaitano, G.; García-Mina, J. M.; Almendros, G.; Gonzàlez-Vila, F. J. Complementary multi-analytical approach to study the distinctive structural features of the main humic fractions in solution: gray humic acid, brown humic acid, and fulvic acid. *J. Agric. Food Chem.* **2009**, *57*, 3266−3272.
(19) Litvin, V. A.; Minaev, B. F.; Baryshnikov, G. V. Synthesis and properties of synthetic fulvic acid derived from hematoxylin. *J. Mol. Struct.* **2015**, *1086*, 25−33.
(20) Fong, S. S.; Seng, L.; Majri, N. B.; Mat, H. B. A comparative evaluation on the oxidative approaches for extraction of humic acids from low rank coal of mukah, sarawak. *J. Braz. Chem. Soc.* **2007**, *18*, 34−40.
(21) Yang, Z.; Gong, L.; Ran, P. Preparation of nitric humic acid by catalytic oxidation from Guizhou coal with catalysts. *Int. J. Min. Sci. Technol.* **2012**, *22*, 75−78.
(22) Mae, K.; Maki, T.; Araki, J.; Miura, K. Extraction of low-rank coals oxidized with hydrogen peroxide in conventionally used solvents at room temperature. *Energy Fuels* **1997**, *11*, 825−831.
(23) Romarís-Hortas, H. V.; Moreda, P. A.; Bermejo-Barrera, P. Application of microwave energy to speed up the alkaline extraction of humic and fulvic acids from marine sediments. *Anal. Chim. Acta* **2007**, *602*, 202−210.
(24) Khanna, R.; Witt, M.; Anwer, M. K.; Agarwal, S. P.; Koch, B. P. Spectroscopic characterization of fulvic acids extracted from the rock exudate Shilajit. *Org. Geochem.* **2008**, *39*, 1719−1724.
(25) Yao, Z.-S.; Wei, X.-Y.; Lv, J.; Liu, F.-J.; Huang, Y.-G.; Xu, J.-J.; Chen, F.-J.; Huang, Y.; Li, Y.; Lu, Y.; Zong, Z.-M. Oxidation of Shenfu Coal with RuO_4 and NaOCl. *Energy Fuels* **2010**, *24*, 1801−1808.
(26) Isoda, T.; Takagi, H.; Kusakabe, K.; Morooka, S. Structural Changes of Alcohol-Solubilized Yallourn Coal in the Hydrogenation over a Ru/Al_2O_3 Catalyst. *Energy Fuels* **1998**, *12*, 503−511.
(27) Raposo, J. C.; Villanueva, U.; Olivares, M.; Madariaga, J. M. Determination of humic substances in sediments by focused ultrasound extraction and ultraviolet visible spectroscopy. *Microchem. J.* **2016**, *128*, 26−33.
(28) Javed, S.; Kohli, K.; Ali, M. Microwave-Assisted Extraction of Fulvic Acid from a Solid Dosage Form: a Statistical Approach. *J. Pharm. Innov.* **2013**, *8*, 175−186.
(29) Ding, M.; Zhao, Y.-P.; Dou, Y.-Q.; Wei, X.-Y.; Fan, X.; Cao, J.-P.; Wang, Y.-L.; Zong, Z.-M. Sequential extraction and thermal dissolution of Shengli lignite. *Fuel Process. Technol.* **2015**, *135*, 20−24.
(30) Li, Z.-K.; Wei, X.-Y.; Yan, H.-L.; Wang, Y.-G.; Kong, J.; Zong, Z.-M. Advances in Lignite Extraction and Conversion under Mild Conditions. *Energy Fuels* **2015**, *29*, 6869−6886.
(31) Yang, F.; Hou, Y.; Wu, W.; Liu, Z. The generation of benzene carboxylic acids from lignite and the change in structural characteristics of the lignite during oxidation. *Fuel* **2017**, *203*, 214−221.
(32) Doskočil, L.; Enev, V.; Pekař, M.; Wasserbauer, J. The spectrometric characterization of lipids extracted from lignite samples from various coal basins. *Org. Geochem.* **2016**, *95*, 34−40.
(33) Feng, L.; Yuan, C.; Mao, L.; Yan, C.; Jiang, X.; Liu, J.; Liu, X. Water occurrence in lignite and its interaction with coal structure. *Fuel* **2019**, *219*, 288−295.
(34) Wang, Z.; Shui, H.; Pan, C.; Li, L.; Ren, S.; Lei, Z.; Kang, S.; Wei, C.; Hu, J. Structural characterization of the thermal extracts of lignite. *Fuel Process. Technol.* **2014**, *120*, 8−15.

https://dx.doi.org/10.1021/acsomega.0c03388
ACS Omega 2020, 5, 27953−27961

(35) Ju, Y.; Yang, S.; Ding, Y.; Sun, C.; Gu, C.; He, Z.; Qin, C.; He, H.; Xu, B. Microwave-enhanced H_2O_2-based process for treating aqueous malachite green solutions: Intermediates and degradation mechanism. *J. Hazard. Mater.* **2009**, *171*, 123−132.
(36) Ahnonkitpanit, E.; Prasassarakich, P. Coal desulphurization in aqueous hydrogen peroxide. *Fuel* **1989**, *68*, 819−824.
(37) Ponte, D. G.; Prieto, I. F.; Viar, P. F.; Luengo, J. C. G. Determination of moisture content in power station coal using microwaves. *Fuel* **1996**, *75*, 133−138.
(38) Guan, Y.; Ma, Y.; Zhang, K.; Chen, H.; Xu, G.; Liu, W.; Yang, Y. Co-pyrolysis behaviors of energy grass and lignite. *Energy Convers. Manage.* **2015**, *93*, 132−140.
(39) Song, Y.; Tahmasebi, A.; Yu, J. Co-pyrolysis of pine sawdust and lignite in a thermogravimetric analyzer and a fixed-bed reactor. *Bioresour. Technol.* **2014**, *174*, 204−211.
(40) Zhang, Y.; Liu, W.; Hu, X.; Zhang, A.; Ma, L.; Shi, Y.; Gong, G. Extraction and Functional Group Characterization of Fulvic Acid from Hami Lignite. *ChemistrySelect* **2019**, *4*, 1448−1455.
(41) Gong, G.; Zhao, Y.; Zhang, Y.; Deng, B.; Liu, W.; Wang, M.; Yuan, X.; Xu, L. Establishment of a molecular structure model for classified products of coal-based fulvic acid. *Fuel* **2020**, *267*, 117210.
(42) Zhao, J.; Xi, B.; Xu, Q.; Zhao, Y.; Wei, Z.; Xu, J.; Zhao, X. Study on fluorescence characteristics of fulvic acid in sediments of Xingkai Lake. *Spectrosc. Spect. Anal.* **2013**, *33*, 1824−1828.
(43) Zou, Y.; Lu, R.; Yang, J. Three-dimensional excitation emission matrix fluorescence spectroscopic characterization of dissolved organic matter in coal mine water. *J. Coal Sci. Eng.* **2012**, *28*, 174−177.

https://dx.doi.org/10.1021/acsomega.0c03388
ACS Omega 2020, 5, 27953−27961